Supplementary Information to

Rovibrational transitions of the methane-water dimer from intermolecular quantum dynamical computations

János Sarka,[1,2] Attila G. Császár,[1,2]
Stuart C. Althorpe,[3] David J. Wales,[3] and Edit Mátyus[1]

[1]*Institute of Chemistry, Eötvös Loránd University, Pázmány Péter sétány 1/A, Budapest, H-1117, Hungary*

[2]*MTA-ELTE Complex Chemical Systems Research Group, P.O. Box 32, H-1518 Budapest 112, Hungary*

[3]*Department of Chemistry, University of Cambridge, Lensfield Road, Cambridge, CB2 1EW, United Kingdom*

(Dated: June 3, 2016)

Contents:

S1. Symmetry analyis (p. 2–11)

S2. A minimum-energy pathway (p. 12)

S3. List of eigenvalues (p. 13–14)

S4. Energy decomposition tables (p. 15–18)

S5. Selected DVR plots (p. 19–20)

S1. SYMMETRY ANALYSIS

We have carried out a symmetry analysis for the methane-water complex, following Dyke's analysis for the water dimer [1].

S1.1. Molecular symmetry group

The permutation-inversion versions generated by the feasible operations obtained by acting on a selected version of the dimer are shown in Figure S1 for all the elements of the molecular symmetry (MS) group. Electronic structure computations consistently show that the global minimum (GM) has C_s symmetry, and thus only half of the structures (24 instead of 48 distinct labeled structures) in Figure S1 represent permutationally distinct minima that are not superimposable by rotation.

The permutation operations of the complex can be obtained by considering the combinations of the permutation operations of the two monomers (there is no proton-proton exchange between the monomers). Dore *et al.* [2] used the character table in Table S8, and we follow their convention for the irreducible representations. (The only difference between Table S8 and the character table of Ref. [2] is the explicit indication of the inversion operations in the present work.) We note that in the notation of Dore *et al.* [2] the even and odd spatial symmetry under the permutation of the water hydrogens is distinguished by the + and − superscripts (and not by the A/B irrep labels in C_{2v}(M) of H_2O). It is important to note that the even and odd character of proton exchange for methane followed by inversion has different subindexes in the + and − blocks.

S1.2. C_s symmetry of the equilibrium structure and tunneling splitting pattern

In this section the irreps of the splitting pattern of a rovibrational state of the dimer are determined. We consider a representation spanned by functions centered in the wells of the distinct versions (Figure S1). Due to the C_s symmetry, there are only 24 distinct wells (instead of 48), and each function, $\phi_n^{\pm}$ ($n = 1, 2, \ldots, 24$), is conveniently chosen to be symmetric (A′) or antisymmetric (A″) with respect to

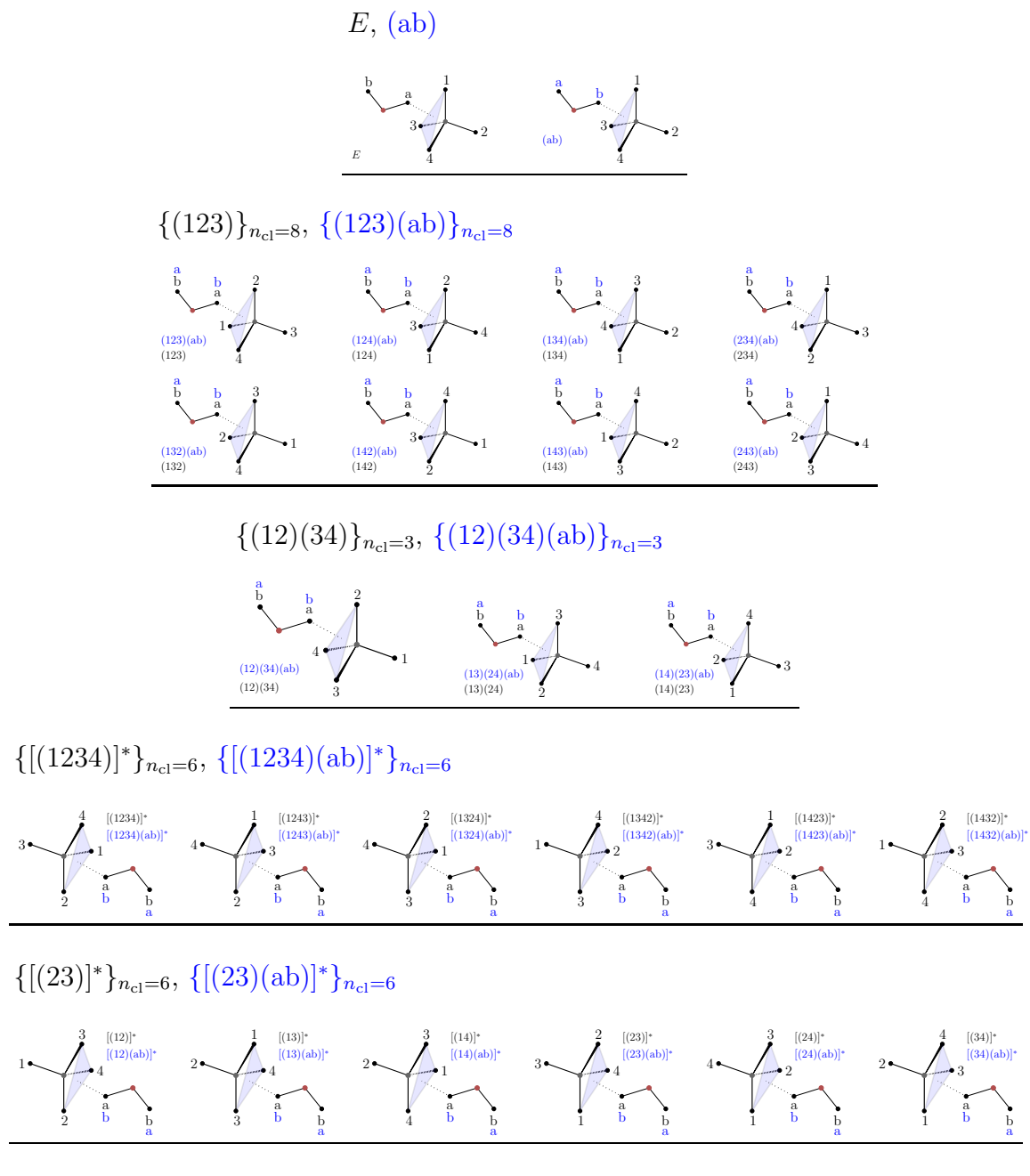

FIG. S1: Mapping for a version of the global minimum structure of the methane-water complex (labeling shown for the identity operation, E) with the elements of the molecular symmetry group, G_{48} given in Table S8.

reflection about the symmetry plane. Thus, the characters of the representations of A′ and A″ symmetries (of the C_s group) can easily be constructed by observing that all the group operations transform one version to another, except for a single element of the $\{[(23)]^*\}_{n_{cl}=6}$ class. For example, if the atomic nuclei are labelled as in the 'parent' version (E) in Figure S1, we notice that it is only the $[(34)]^*$ operation that leaves it invariant up to a 180° rotation. There are four different permutation-

G_{48}	E	...		...	$[(23)]^*$
$n_{\rm cl}$	1	...		...	6
$\Gamma_{\rm A'}$	24	0	...	0	4
$\Gamma_{\rm A''}$	24	0	...	0	-4

TABLE S1: Characters of the elements of G_{48} spanned by the symmetric, A′ (C_s), and anti-symmetric, A″ (C_s), representations. The A′ and A″ representations are composed of C_s symmetric and C_s anti-symmetric functions centered at the rotationally non-superimposable permutation-inversion versions of the plane-symmetric global minimum of the CH_4·H_2O complex.

inversion versions (which reserve the parity of the CH_4 moiety) that are left invariant (up to a 180° rotation) by only one of the operations in the $\{[(23)]^*\}_{n_{\rm cl}=6}$ class. With this reasoning we obtain the characters of the A′ and A″ representations listed in Table S1. The A′ and A″ representations can be decomposed into a direct sum of irreducible representations of the G_{48} molecular symmetry group (see Table S8) as

$$\Gamma_{\rm A'} = {\rm A}_1^+ \oplus {\rm E}^+ \oplus {\rm F}_1^+ \oplus 2{\rm F}_2^+ \oplus {\rm A}_2^- \oplus {\rm E}^- \oplus 2{\rm F}_1^- \oplus {\rm F}_2^- \tag{S1}$$

$$\Gamma_{\rm A''} = {\rm A}_2^+ \oplus {\rm E}^+ \oplus 2{\rm F}_1^+ \oplus {\rm F}_2^+ \oplus {\rm A}_1^- \oplus {\rm E}^- \oplus {\rm F}_1^- \oplus 2{\rm F}_2^-. \tag{S2}$$

We assume that the tunneling splitting of the zero-point vibration with $J = 0$ corresponds to the $\Gamma_{\rm A'}$ representation (see Eq. (5) of the main text), and thus the symmetry of the zero-point vibrational (ZPV) splitting manifold is given by Eq. (S1). For certain excited vibrational states (anti-symmetric with respect to the symmetry plane of the equilibrium structure) or for a totally symmetric vibrational state with $J > 0$ irreps in Eq. (S2) also become accessible.

S1.3. Spin functions

In order to determine which irreps of the spatial wave function are allowed by the Pauli principle, we consider the representation of G_{48} spanned by all the primitive spin functions of the hydrogens of CH_4·H_2O. Altogether $2^4 \cdot 2^2 = 64$ spin functions can be constructed for the protons, $(\sigma\sigma\sigma\sigma).(\sigma\sigma')$, where $\sigma = \alpha, \beta$ labels a proton spin function of CH_4 and $\sigma' = \alpha', \beta'$ is the spin function of a proton in the H_2O moiety. The characters of this representation span by all possible spin functions

G_{48}	E	(123)	(14)(23)	[(1423)(ab)]*	[(23)(ab)]*	(ab)	(123)(ab)	(14)(23)(ab)	[(1423)]*	[(23)]*
$n_{\rm cl}$	1	8	3	6	6	1	8	3	6	6
$\Gamma_{\rm spin}$	64	16	16	4	16	32	8	8	8	32

TABLE S2: Characters of the classes of G_{48} for the representation spanned by the elementary spin functions of the protons in $CH_4{\cdot}H_2O$.

can be constructed by observing that only those functions contribute to the trace of the representation matrix of a symmetry operation that contain the same spin functions for the particles included in a permutation cycle (the inversion does not have any effect on the spin functions). For example, the character of (123) is obtained by counting the number of functions left invariant, which must have the form $(\alpha\alpha\alpha/\beta\beta\beta)(\alpha/\beta)(\alpha'/\beta')(\alpha'/\beta')$, producing $2^4 = 16$ possibilities.

The 64-dimensional spin representation, Table S2, is reducible to the direct sum

$$\Gamma_{\rm spin} = 15\mathrm{A}_1^+ \oplus 3\mathrm{E}^+ \oplus 9\mathrm{F}_2^+ \oplus 5\mathrm{A}_2^- \oplus 1\mathrm{E}^- \oplus 3\mathrm{F}_1^- \quad (\text{in } G_{48}). \tag{S3}$$

We note that the same result could have been obtained by forming a direct product of the symmetry-adapted spin functions of CH_4 and H_2O (there are no exchanges between the methane and water moieties in the MS group). The 64-dimensional representation of the elements of the MS group of CH_4, $T_{\rm d}(\mathrm{M})$, would reduce to the direct sum

$$\Gamma_{\rm spin} = 4 \cdot (5\mathrm{A}_1 \oplus \mathrm{E} \oplus 3\mathrm{F}_2) \quad (\text{in } T_{\rm d}(\mathrm{M})). \tag{S4}$$

The symmetry-adapted spin functions can also be constructed and characterized with the total spin quantum number, I, and with its projection to the laboratory-fixed Z axis, m_I. The $5\mathrm{A}_1$ functions have $I = 2$, $m_I = -2, -1, 0, 1, 2$. There are three sets of functions with $I = 1$, $m_I = -1, 0, 1$ corresponding to F_2 and a degenerate pair of $I = 0, m_I = 0$ functions, according to the didactic explanation of Ref. [3].

If we consider the permutation group of two elements for the protons of water and label the symmetric and the antisymmetric representations with A^+ and A^- (we choose this notation to arrive at a labeling convention similar to G_{48} introduced

TABLE S3: Symmetry decomposition of the direct product of two irreps in the G_{48} group (Table S8).

$\otimes$	A_1^+	A_2^+	E^+	F_1^+	F_2^+	A_1^-	A_2^-	E^-	F_1^-	F_2^-
A_1^+	A_1^+	A_2^+	E^+	F_1^+	F_2^+	A_1^-	A_2^-	E^-	F_1^-	F_2^-
A_2^+	A_2^+	A_1^+	E^+	F_2^+	F_1^+	A_2^-	A_1^-	E^-	F_2^-	F_1^-
E^+	E^+	E^+	$A_1^+ \oplus A_2^+ \oplus E^+$	$F_1^+ \oplus F_2^+$	$F_1^+ \oplus F_2^+$	E^-	E^-	$A_1^- \oplus A_2^- \oplus E^-$	$F_1^- \oplus F_2^-$	$F_1^- \oplus F_2^-$
F_1^+	F_1^+	F_2^+	$F_1^+ \oplus F_2^+$	$A_1^+ \oplus E^+ \oplus F_1^+ \oplus F_2^+$	$A_2^+ \oplus E^+ \oplus F_1^+ \oplus F_2^+$	F_1^-	F_2^-	$F_1^- \oplus F_2^-$	$A_1^- \oplus E^- \oplus F_1^- \oplus F_2^-$	$A_2^- \oplus E^- \oplus F_1^- \oplus F_2^-$
F_2^+	F_2^+	F_1^+	$F_1^+ \oplus F_2^+$	$A_2^+ \oplus E^+ \oplus F_1^+ \oplus F_2^+$	$A_1^+ \oplus E^+ \oplus F_1^+ \oplus F_2^+$	F_2^-	F_1^-	$F_1^- \oplus F_2^-$	$A_2^- \oplus E^- \oplus F_1^- \oplus F_2^-$	$A_1^- \oplus E^- \oplus F_1^- \oplus F_2^-$
A_1^-	A_1^-	A_2^-	E^-	F_1^-	F_2^-	A_1^+	A_2^+	E^+	F_1^+	F_2^+
A_2^-	A_2^-	A_1^-	E^-	F_2^-	F_1^-	A_2^+	A_1^+	E^+	F_2^+	F_1^+
E^-	E^-	E^-	$A_1^- \oplus A_2^- \oplus E^-$	$F_1^- \oplus F_2^-$	$F_1^- \oplus F_2^-$	E^+	E^+	$A_1^+ \oplus A_2^+ \oplus E^+$	$F_1^+ \oplus F_2^+$	$F_1^+ \oplus F_2^+$
F_1^-	F_1^-	F_2^-	$F_1^- \oplus F_2^-$	$A_1^- \oplus E^- \oplus F_1^- \oplus F_2^-$	$A_2^- \oplus E^- \oplus F_1^- \oplus F_2^-$	F_1^+	F_2^+	$F_1^+ \oplus F_2^+$	$A_1^+ \oplus E^+ \oplus F_1^+ \oplus F_2^+$	$A_2^+ \oplus E^+ \oplus F_1^+ \oplus F_2^+$
F_2^-	F_2^-	F_1^-	$F_1^- \oplus F_2^-$	$A_2^- \oplus E^- \oplus F_1^- \oplus F_2^-$	$A_1^- \oplus E^- \oplus F_1^- \oplus F_2^-$	F_2^+	F_1^+	$F_1^+ \oplus F_2^+$	$A_2^+ \oplus E^+ \oplus F_1^+ \oplus F_2^+$	$A_1^+ \oplus E^+ \oplus F_1^+ \oplus F_2^+$

in Ref. [2]), we obtain:

$$\Gamma_{\text{spin}} = 16 \cdot (3\mathrm{A}^+ \oplus \mathrm{A}^-) \quad (\text{in } S_2). \tag{S5}$$

The three spin functions of A^+ symmetry correspond to $I' = 1, m_{I'} = -1, 0, 1$ (ortho-H_2O) and the spin function of A^- symmetry has $I' = 0, m_{I'} = 0$ (para-H_2O). We note that Eqs. (S4) and (S5) are indeed in agreement with Eq. (S3), and we conclude that the spin functions belonging to Γ^+ irreps correspond to ortho-H_2O, whereas the spin functions in the Γ^- irreps correspond to para-H_2O.

S1.4. Spin-statistical weights

The Fermi–Dirac statistics (the 'Pauli principle' for fermions) requires that the total wave function remains invariant under the effect of even permutations, and changes sign under odd permutation operations (only 'pure' permutations and not permutation-inversions need to be considered). Since the MS group of methane does not contain any odd permutations (only odd permutation-inversion operations), we observe that both the A_1 and A_2 irreps satisfy the Pauli principle for methane. When the permutation of the protons of the H_2O moiety is also considered, we conclude that the total wave function satisfies Fermi–Dirac statistics if it transforms as the A_1^- or A_2^- irreps of G_{48}. Table S4 lists the combinations of the spatial and the spin functions that satisfy this requirement (we also used the irrep multiplication table, Table S3), and it also contains the spin statistical weights, which were calculated by considering the number of spin functions of a given species.

TABLE S4: Spin-statistical weights, n_{sw}, of the spatial functions of $CH_4{\cdot}H_2O$.

$\Gamma_{\mathrm{spatial}}$	$n_{\Gamma_i}\Gamma_{\mathrm{spin}}$	$\Gamma_{\mathrm{spatial}} \otimes n_{\Gamma_i}\Gamma_{\mathrm{spin}}$	$n_{\mathrm{sw}} = n_{\mathrm{A_1^-}} + n_{\mathrm{A_2^-}}$	ortho/para
A_1^+	$0A_1^-$ $5A_2^-$	$A_1^+ \otimes 0A_1^- = 0A_1^-$ $A_1^+ \otimes 5A_2^- = 5A_2^-$	5	para
A_2^+	$5A_2^-$ $0A_1^-$	$A_2^+ \otimes 5A_2^- = 5A_1^-$ $A_2^+ \otimes 0A_1^- = 0A_2^-$	5	para
E^+	$1E^-$	$E^+ \otimes 1E^- = A_1^- \oplus A_2^- \oplus E^-$	2	para
F_1^+	$3F_1^-$ $0F_2^-$	$F_1^+ \otimes 3F_1^- = 3(A_1^- \oplus E^- \oplus F_1^- \oplus F_2^-)$ $F_1^+ \otimes 0F_2^- = 0(A_2^- \oplus E^- \oplus F_1^- \oplus F_2^-)$	3	para
F_2^+	$0F_2^-$ $3F_1^-$	$F_2^+ \otimes 0F_2^- = 0(A_1^- \oplus E^- \oplus F_1^- \oplus F_2^-)$ $F_2^+ \otimes 3F_1^- = 3(A_2^- \oplus E^- \oplus F_1^- \oplus F_2^-)$	3	para
A_1^-	$15A_1^+$ $0A_2^+$	$A_1^- \otimes 15A_1^+ = 15A_1^-$ $A_1^- \otimes 0A_2^+ = 0A_2^-$	15	ortho
A_2^-	$0A_2^+$ $15A_1^+$	$A_2^- \otimes 0A_2^+ = 0A_1^-$ $A_2^- \otimes 15A_1^+ = 15A_2^-$	15	ortho
E^-	$3E^+$	$E^- \otimes 3E^+ = 3(A_1^- \oplus A_2^- \oplus E^-)$	6	ortho
F_1^-	$0F_1^+$ $9F_2^+$	$F_1^- \otimes 0F_1^+ = 0(A_1^- \oplus E^- \oplus F_1^- \oplus F_2^-)$ $F_1^- \otimes 9F_2^+ = 9(A_2^- \oplus E^- \oplus F_1^- \oplus F_2^-)$	9	ortho
F_2^-	$9F_2^+$ $0F_1^+$	$F_2^- \otimes 9F_2^+ = 9(A_1^- \oplus E^- \oplus F_1^- \oplus F_2^-)$ $F_2^- \otimes 0F_1^+ = 0(A_2^- \oplus E^- \oplus F_1^- \oplus F_2^-)$	9	ortho

S1.5. Selection rules for electric dipole transitions

Similarly to Dyke's reasoning for the water dimer [1], we can identify the symmetry species corresponding to the projection of the molecular electric dipole moment along an axis fixed in space by identifying the irrep that is invariant to the permutation of identical nuclei but changes sign under inversion. Hence, $-\boldsymbol{\mu} \cdot \boldsymbol{E}$ transforms like A_2^+ in G_{48} and any transition is allowed that connects initial, 'i', and final, 'f', states with the same spin function and for which the transition moment with the initial and final spatial functions is non-vanishing:

$$\langle \chi_{\mathrm{spin,f}} | \chi_{\mathrm{spin,i}} \rangle \neq 0 \tag{S6}$$

and

$$\Gamma_{\text{spatial,f}} \otimes \mathrm{A}_2^+ \otimes \Gamma_{\text{spatial,i}} \supset \mathrm{A}_1^+ \quad \Leftrightarrow \quad \Gamma_{\text{spatial,f}} \otimes \Gamma_{\text{spatial,i}} \supset \mathrm{A}_2^+. \tag{S7}$$

Therefore, an electric dipole transition can be allowed between pairs of states, f $\leftrightarrow$ i, of the following symmetries

$$\mathrm{A}_1^\pm \leftrightarrow \mathrm{A}_2^\pm \quad \text{or} \quad \mathrm{F}_1^\pm \leftrightarrow \mathrm{F}_2^\pm \quad \text{or} \quad \mathrm{E}^\pm \leftrightarrow \mathrm{E}^\pm \tag{S8}$$

From Table S4 we see that the spatial states connected by an electric dipole transition, Eq. (S8), have exactly the same set of spin functions allowed by the Fermi–Dirac statistics. Hence the spin statistical weight of each transition equals the statistical weight, n_{sw}, of the initial (and the final) state.

S1.6. The case of a near symmetric rotor

Our symmetry analysis has been exact up to this point. The CH_4·H_2O dimer, similarly to the water dimer, is a near prolate symmetric top, the rotational constants of the global minimum structure of the main text are

$$A_{\text{e}} = 4.229 \text{ cm}^{-1} \gg B_{\text{e}} = 0.159 \text{ cm}^{-1} \approx C_{\text{e}} = 0.158 \text{ cm}^{-1}. \tag{S9}$$

In this subsection we discuss the symmetry consequences of the near-symmetric rotor character of the methane-water complex by noting that K is nearly a good quantum number (corresponding to the projection of the rotational angular momentum onto the molecular near symmetry axis).

For this purpose, we define the (right-handed) body-fixed (BF) frame by choosing the z axis going from the center of mass of H_aH_bO to the center of mass of $CH_1H_2H_3H_4$. The y axis is fixed by the bisector of H_aH_bO and points towards the center of mass of H_aH_b. (We note that this BF frame cannot be defined if the bisector is parallel with the z axis.) In Table S5 we collect the transformation properties of this BF frame, and the corresponding Euler angles and symmetrized rotational

TABLE S5: Transformation properties of the the body-fixed frame and the corresponding Euler angles and Wang functions upon the permutation-inversion operations of $CH_4{\cdot}H_2O$ in G_{48}.

G_{48}	E	(123)	(14)(23)	[(1423)(ab)]*	[(23)(ab)]*	(ab)	(123)(ab)	(14)(23)(ab)	[(1423)]*	[(23)]*	
$n_{\rm cl}$	1	8	3	6	6	1	8	3	6	6	
BF transf. [a]	E	E	E	$R_x(\pi)$ [b]	$R_x(\pi)$ [b]	E	E	E	$R_x(\pi)$ [b]	$R_x(\pi)$ [b]	
(α,β,γ)	(α,β,γ)	(α,β,γ)	(α,β,γ)	$(\pi+\alpha,\pi-\beta,-\gamma)$	$(\pi+\alpha,\pi-\beta,-\gamma)$	(α,β,γ)	(α,β,γ)	(α,β,γ)	$(\pi+\alpha,\pi-\beta,-\gamma)$	$(\pi+\alpha,\pi-\beta,-\gamma)$	
$D^{(J),*}_{M,K}$	$D^{(J),*}_{M,K}$	$D^{(J),*}_{M,K}$	$D^{(J),*}_{M,K}$	$(-1)^J D^{(J),*}_{M,-K}$	$(-1)^J D^{(J),*}_{M,-K}$	$D^{(J),*}_{M,K}$	$D^{(J),*}_{M,K}$	$D^{(J),*}_{M,K}$	$(-1)^J D^{(J),*}_{M,-K}$	$(-1)^J D^{(J),*}_{M,-K}$	
$\Gamma(\Psi^{(\pm)}_{JKM})$:											
J even, $K=0$	1	1	1	1	1	1	1	1	1	1	A_1^+
J odd, $K=0$	1	1	1	−1	−1	1	1	1	−1	−1	A_2^+
J even, $K\neq 0$, $\Psi^{(+)}$	1	1	1	1	1	1	1	1	1	1	A_1^+
J odd, $K\neq 0$, $\Psi^{(+)}$	1	1	1	−1	−1	1	1	1	−1	−1	A_2^+
J even, $K\neq 0$, $\Psi^{(-)}$	1	1	1	−1	−1	1	1	1	−1	−1	A_2^+
J odd, $K\neq 0$, $\Psi^{(-)}$	1	1	1	1	1	1	1	1	1	1	A_1^+

[a]: BF transf: the rotational operation corresponding to the change in orientation of the body-fixed frame (BF) described in the text.
[b]: $R_x(\pi)$ is a 180° rotation of the body-fixed frame around the x axis.

Wang functions

$$\Psi_{J0M} = D^{(J),*}_{M,0}(\alpha,\beta,\gamma) \tag{S10}$$

$$\Psi^{(\pm)}_{JKM} = \frac{1}{\sqrt{2}}\left(D^{(J),*}_{M,K}(\alpha,\beta,\gamma) \pm D^{(J),*}_{M,-K}(\alpha,\beta,\gamma)\right) \quad (K\geq 1). \tag{S11}$$

According to Table S5, the approximate symmetry assignment for the rotational functions of $CH_4{\cdot}H_2O$ using the symmetric rotor eigenfunctions, $\Psi^{(\pm)}_{JKM}$, with the quantum number K, which is nearly exact for (the near prolate) $CH_4{\cdot}H_2O$, is

$$\begin{aligned}
A_1^+ :\quad & J=0,\\
& J \text{ even and } K=0,\\
& J \text{ even and } K\neq 0 \text{ and } \Psi^{(+)},\\
& J \text{ odd and } K\neq 0 \text{ and } \Psi^{(-)}
\end{aligned} \tag{S12}$$

$$\begin{aligned}
A_2^+ :\quad & J \text{ odd and } K=0,\\
& J \text{ odd and } K\neq 0 \text{ and } \Psi^{(+)},\\
& J \text{ even and } K\neq 0 \text{ and } \Psi^{(-)}.
\end{aligned} \tag{S13}$$

By comparing this result with the electric dipole selection rules, Eqs. (S6)–(S8), which allow transitions between rovibrational levels of symmetries related by

$\Gamma_{\text{spatial,f/i}} = \Gamma_{\text{spatial,i/f}} \otimes \text{A}_2^+$, we conclude that this selection rule simplifies to the requirement that the appropriate rovibrational transitions connect levels of the *same vibrational symmetry*. Table S4 shows that the same spin functions can be assigned to the 'i' and 'f' spatial functions related by this relationship; thus, the spin selection rule, Eq. (S6), is automatically satisfied.

TABLE S6: Character table of the molecular symmetry group of H_2O (Table A-5 in [4]).

$C_{2v}(M)$	E	(ab)	E^*	$[(ab)]^*$
n_{cl}	1	1	1	1
A_1	1	1	1	1
A_2	1	1	−1	−1
B_1	1	−1	−1	1
B_2	1	−1	1	−1

TABLE S7: Character table of the molecular symmetry group of CH_4 (Table A-14 in [4]).

$T_d(M)$	E	(123)	(14)(23)	$[(1423)]^*$	$[(23)]^*$
n_{cl}	1	8	6	6	
A_1	1	1	1	1	1
A_2	1	1	1	−1	−1
E	2	−1	2	0	0
F_1	3	0	−1	1	−1
F_2	3	0	−1	−1	1

TABLE S8: Character table of the molecular symmetry group of $CH_4{\cdot}H_2O$, G_{48} (the table is taken from Ref. [2] but with explicit notation for space inversion). The green dashed box indicates the subgroup of elements without inversion, G_{24}, and their corresponding irreps are the same as those of the full group but without the 1 and 2 subscripts.

G_{48}	E	(123)	(14)(23)	$[(1423)(ab)]^*$	$[(23)(ab)]^*$	(ab)	(123)(ab)	(14)(23)(ab)	$[(1423)]^*$	$[(23)]^*$
n_{cl}	1	8	3	6	6	1	8	3	6	6
A_1^+	1	1	1	1	1	1	1	1	1	1
A_2^+	1	1	1	−1	−1	1	1	1	−1	−1
E^+	2	−1	2	0	0	2	−1	2	0	0
F_1^+	3	0	−1	1	−1	3	0	−1	1	−1
F_2^+	3	0	−1	−1	1	3	0	−1	−1	1
A_1^-	1	1	1	1	1	−1	−1	−1	−1	−1
A_2^-	1	1	1	−1	−1	−1	−1	−1	1	1
E^-	2	−1	2	0	0	−2	1	−2	0	0
F_1^-	3	0	−1	1	−1	−3	0	1	−1	1
F_2^-	3	0	−1	−1	1	−3	0	1	1	−1

S2. A MINIMUM-ENERGY PATHWAY

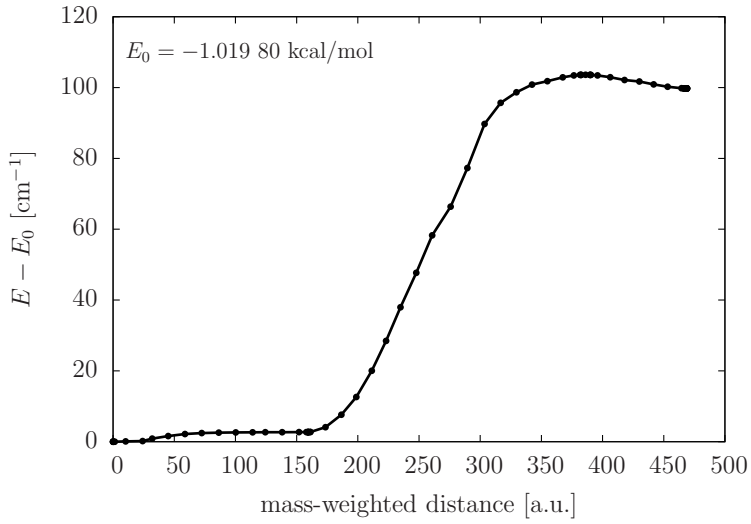

FIG. S2: Minimum-energy pathway connecting the global and the secondary minima on the AOSz05 PES [5].

S3. LIST OF EIGENVALUES

TABLE S9: The first 70 $J = 0$ vibrational energy levels of the CH_4·H_2O dimer computed with the GENIUSH code using the AOSz05 PES [5] and the QCHB15 PES [6] with two different basis sets. The zero-point vibrational energies (ZPVE) are reported first, all other energy values are relative to the ZPVE values. All values are in cm^{-1}. SG refers to the smaller grid described in Section 2. A larger grid (LG) is obtained from SG by using 101 unscaled Legendre DVR points for the $q_5 = \cos\beta$ degree of freedom.

	AOSz05 [5]		QCHB15 [6]			AOSz05 [5]		QCHB15 [6]	
J0.n	$\tilde{\nu}$(SG)	$\tilde{\nu}$(LG)	$\tilde{\nu}$(SG)	$\tilde{\nu}$(LG)	J0.n	$\tilde{\nu}$(SG)	$\tilde{\nu}$(LG)	$\tilde{\nu}$(SG)	$\tilde{\nu}$(LG)
1	206.792	206.801	215.637	215.642	36	48.672	48.685	48.215	48.328
2	4.763	4.763	4.584	4.587	37	50.514	50.628	51.933	52.058
3	4.763	4.764	4.584	4.588	38	50.514	50.628	51.933	52.058
4	4.765	4.764	4.596	4.588	39	50.620	50.632	52.043	52.064
5	6.930	6.934	7.059	7.062	40	53.260	53.328	52.200	52.237
6	11.177	11.190	11.084	11.087	41	53.260	53.329	52.205	52.240
7	11.193	11.192	11.088	11.090	42	53.315	53.329	52.205	52.240
8	11.193	11.192	11.088	11.090	43	53.935	53.977	54.499	54.532
9	28.919	29.001	30.338	30.422	44	54.039	54.095	55.553	55.617
10	28.938	29.002	30.350	30.423	45	54.039	54.095	55.553	55.617
11	28.938	29.002	30.350	30.423	46	54.108	54.097	55.622	55.619
12	32.600	32.630	32.383	32.388	47	56.540	56.650	57.486	57.630
13	32.600	32.630	32.383	32.388	48	56.540	56.651	57.486	57.631
14	32.614	32.630	32.387	32.391	49	56.652	56.651	57.650	57.631
15	32.701	32.705	32.562	32.578	50	61.393	61.669	61.494	61.684
16	32.701	32.705	32.562	32.579	51	61.393	61.669	61.494	61.684
17	32.708	32.708	32.565	32.579	52	61.490	61.677	61.691	61.693
18	34.407	34.405	35.827	35.834	53	61.490	61.687	62.397	62.703
19	35.740	35.880	36.287	36.369	54	61.673	61.687	62.397	62.703
20	35.740	35.880	36.287	36.369	55	61.690	61.694	62.686	62.710
21	36.257	36.317	36.346	36.428	56	63.441	63.460	65.358	65.429
22	36.257	36.317	36.346	36.428	57	63.441	63.460	65.675	65.710
23	36.323	36.322	36.486	36.530	58	64.196	64.168	65.675	65.710
24	36.365	36.397	36.486	36.530	59	64.514	64.576	65.835	65.818
25	36.365	36.397	36.535	36.536	60	65.631	65.821	66.060	66.133
26	41.102	41.104	41.599	41.598	61	65.744	65.823	66.065	66.137
27	41.102	41.105	41.599	41.600	62	65.744	65.823	66.118	66.137
28	41.125	41.105	41.603	41.600	63	65.992	66.070	66.118	66.281
29	45.766	45.916	46.982	47.071	64	66.053	66.075	66.219	66.284
30	45.827	45.916	47.008	47.123	65	66.071	66.075	66.219	66.284
31	45.827	45.917	47.008	47.123	66	66.071	66.156	66.365	66.475
32	47.156	47.253	47.056	47.125	67	71.052	71.303	70.355	70.625
33	47.156	47.253	47.498	47.536	68	71.261	71.309	70.589	70.632
34	47.966	48.000	47.498	47.536	69	71.261	71.309	70.589	70.632
35	47.966	48.000	48.215	48.328	70	71.910	72.132	72.772	72.987

TABLE S10: The first 150 $J = 1$ and 2 rovibrational energy levels of the CH_4·H_2O dimer computed with the GENIUSH code using the AOSz05 PES [5]. The zero-point vibrational energies (ZPVE) are reported first, all other energy values are relative to the ZPVE values. All values are given in cm^{-1}.

$J = 1$						$J = 2$					
J1.n	$\tilde{\nu}$	J1.n	$\tilde{\nu}$	J1.n	$\tilde{\nu}$	J2.n	$\tilde{\nu}$	J2.n	$\tilde{\nu}$	J2.n	$\tilde{\nu}$
1	0.289	51	36.007	101	51.353	1	0.867	51	31.157	101	43.539
2	5.044	52	36.007	102	53.514	2	5.605	52	31.202	102	43.550
3	5.044	53	36.542	103	53.514	3	5.607	53	31.202	103	45.246
4	5.045	54	36.542	104	53.567	4	5.607	54	32.764	104	45.309
5	7.219	55	36.609	105	54.070	5	7.796	55	32.764	105	45.341
6	7.905	56	36.649	106	54.085	6	8.485	56	32.770	106	45.341
7	7.909	57	36.649	107	54.135	7	8.490	57	32.770	107	45.477
8	7.911	58	38.926	108	54.135	8	8.490	58	32.788	108	45.477
9	7.911	59	38.926	109	54.174	9	8.497	59	32.788	109	46.677
10	7.915	60	40.331	110	54.174	10	8.501	60	33.464	110	46.741
11	7.915	61	40.331	111	54.207	11	8.501	61	33.464	111	46.741
12	11.457	62	40.376	112	54.334	12	12.019	62	33.480	112	47.132
13	11.475	63	40.376	113	54.334	13	12.039	63	33.571	113	47.132
14	11.475	64	40.379	114	54.389	14	12.039	64	33.571	114	48.009
15	13.113	65	40.380	115	54.430	15	13.682	65	33.578	115	48.009
16	13.113	66	41.381	116	54.439	16	13.682	66	34.185	116	48.808
17	14.543	67	41.381	117	54.470	17	15.120	67	34.185	117	48.808
18	14.543	68	41.404	118	54.470	18	15.120	68	34.187	118	49.496
19	14.552	69	42.998	119	54.476	19	15.130	69	34.187	119	49.603
20	14.554	70	43.001	120	54.476	20	15.136	70	34.188	120	49.606
21	14.555	71	44.728	121	54.571	21	15.136	71	34.188	121	49.606
22	14.555	72	44.750	122	54.571	22	15.137	72	35.210	122	49.620
23	19.329	73	44.809	123	56.813	23	19.895	73	36.540	123	49.814
24	19.329	74	44.809	124	56.813	24	19.895	74	36.540	124	49.814
25	26.361	75	44.933	125	56.921	25	23.320	75	37.111	125	50.858
26	26.363	76	44.933	126	56.965	26	23.320	76	37.111	126	50.858
27	29.189	77	46.071	127	56.965	27	26.374	77	37.180	127	51.233
28	29.209	78	46.133	128	57.216	28	26.374	78	37.217	128	51.233
29	29.209	79	46.133	129	57.216	29	26.375	79	37.217	129	51.326
30	29.427	80	46.568	130	57.239	30	26.375	80	37.479	130	51.839
31	29.433	81	46.568	131	57.262	31	26.388	81	37.479	131	51.866
32	29.729	82	47.440	132	57.262	32	26.388	82	37.537	132	51.866
33	29.731	83	47.440	133	57.265	33	26.937	83	37.537	133	51.946
34	29.760	84	48.247	134	59.296	34	26.944	84	37.546	134	51.963
35	29.760	85	48.247	135	59.315	35	29.662	85	37.546	135	51.963
36	29.765	86	48.946	136	61.438	36	29.662	86	37.564	136	52.163
37	29.765	87	49.058	137	61.449	37	29.730	87	37.564	137	52.163
38	30.474	88	49.058	138	61.634	38	29.752	88	38.531	138	52.191
39	30.474	89	49.060	139	61.634	39	29.752	89	38.531	139	52.191
40	30.588	90	49.065	140	61.663	40	29.995	90	39.505	140	52.227
41	30.588	91	49.266	141	61.663	41	30.012	91	39.505	141	52.228
42	30.633	92	49.266	142	61.715	42	30.294	92	40.883	142	54.022
43	30.633	93	50.749	143	61.715	43	30.301	93	40.883	143	54.022
44	32.888	94	50.749	144	61.839	44	30.328	94	40.928	144	54.071
45	32.888	95	50.848	145	61.839	45	30.328	95	40.928	145	54.590
46	32.902	96	51.283	146	61.952	46	30.336	96	40.928	146	54.634
47	32.991	97	51.310	147	61.984	47	30.336	97	40.933	147	54.642
48	32.991	98	51.310	148	62.975	48	31.043	98	41.939	148	54.720
49	32.998	99	51.326	149	62.975	49	31.043	99	41.939	149	54.750
50	34.675	100	51.353	150	63.179	50	31.157	100	41.963	150	54.909

S4. ENERGY DECOMPOSITION TABLES

For the present study, we introduced a very simple energy decomposition scheme to better understand the tunneling splitting manifold. Using the short-hand notation $\langle\hat{O}\rangle_{J,i} = \langle\Psi^{\rm rv}_{J,i}|\hat{O}|\Psi^{\rm rv}_{J,i}\rangle$, we write the rovibrational energy corresponding to the $\Psi^{\rm rv}_{J,i}$ wave function as a sum

$$E^{\rm rv}_{J,i} = \langle\Psi^{\rm rv}_{J,i}|\hat{H}|\Psi^{\rm rv}_{J,i}\rangle = \langle\hat{T}\rangle_{J,i} + \langle\hat{V}\rangle_{J,i} \tag{S14}$$

To trace high excitations of the rotational monomer states, and separate them from 'non-spinning' monomer states, we further partition the kinetic energy terms as

$$\begin{aligned}
\langle\hat{T}\rangle_{J,i} &= \langle\hat{T}^{\rm v}\rangle_{J,i} + \langle\hat{T}^{\rm rv}\rangle_{J,i} + \langle\hat{T}^{\rm r}\rangle_{J,i} \\
&= \langle\hat{T}^{\rm v}_{R}\rangle_{J,i} + \boxed{\langle\hat{T}^{\rm v}_{\theta,\phi}\rangle_{J,i}} + \boxed{\langle\hat{T}^{\rm v}_{\alpha,\beta,\gamma}\rangle_{J,i}} + \langle\hat{T}^{\rm v}_{\rm cpl}\rangle_{J,i} \\
&+ \langle\hat{T}^{\rm rv}_{R}\rangle_{J,i} + \underbrace{\boxed{\langle\hat{T}^{\rm rv}_{\theta,\phi}\rangle_{J,i}}}_{\rm H_2O} + \underbrace{\boxed{\langle\hat{T}^{\rm rv}_{\alpha,\beta,\gamma}\rangle_{J,i}}}_{\rm CH_4} + \langle\hat{T}^{\rm rv}_{\rm cpl}\rangle_{J,i} + \langle\hat{T}^{\rm r}\rangle_{J,i}
\end{aligned} \tag{S15}$$

Using the GENIUSH program, these energy contributions are obtained in a post-processing step for the calculated eigenvectors (wave functions). This post-processing step amounts to a single matrix multiplication of the computed eigenvectors used as a trial vector with the highlighted terms of the Hamiltonian matrix, and then forming the scalar product of the product vector with the original one.

Figures S3, S4, and S5 show the result of the energy decomposition by visualizing the energy contribution of the different terms (and hence different rotors) of the Hamiltonian to the total rovibrational energy of variationally computed energy levels of the complex with $J = 0, 1$, and 2, respectively. First of all, we observe in these figures that the potential energy contributions as well as the kinetic energy contributions of the intermolecular stretching exhibit very small variations over the studied energy range. However, there are more significant variations in the kinetic energy contributions to the angular part of the water and the methane monomers and in the kinetic energy coupling terms.

Although in GENIUSH we use numerical kinetic energy operators constructed on the fly, the analytic form of the Hamiltonian of two coupled polyatomic molecules [7]

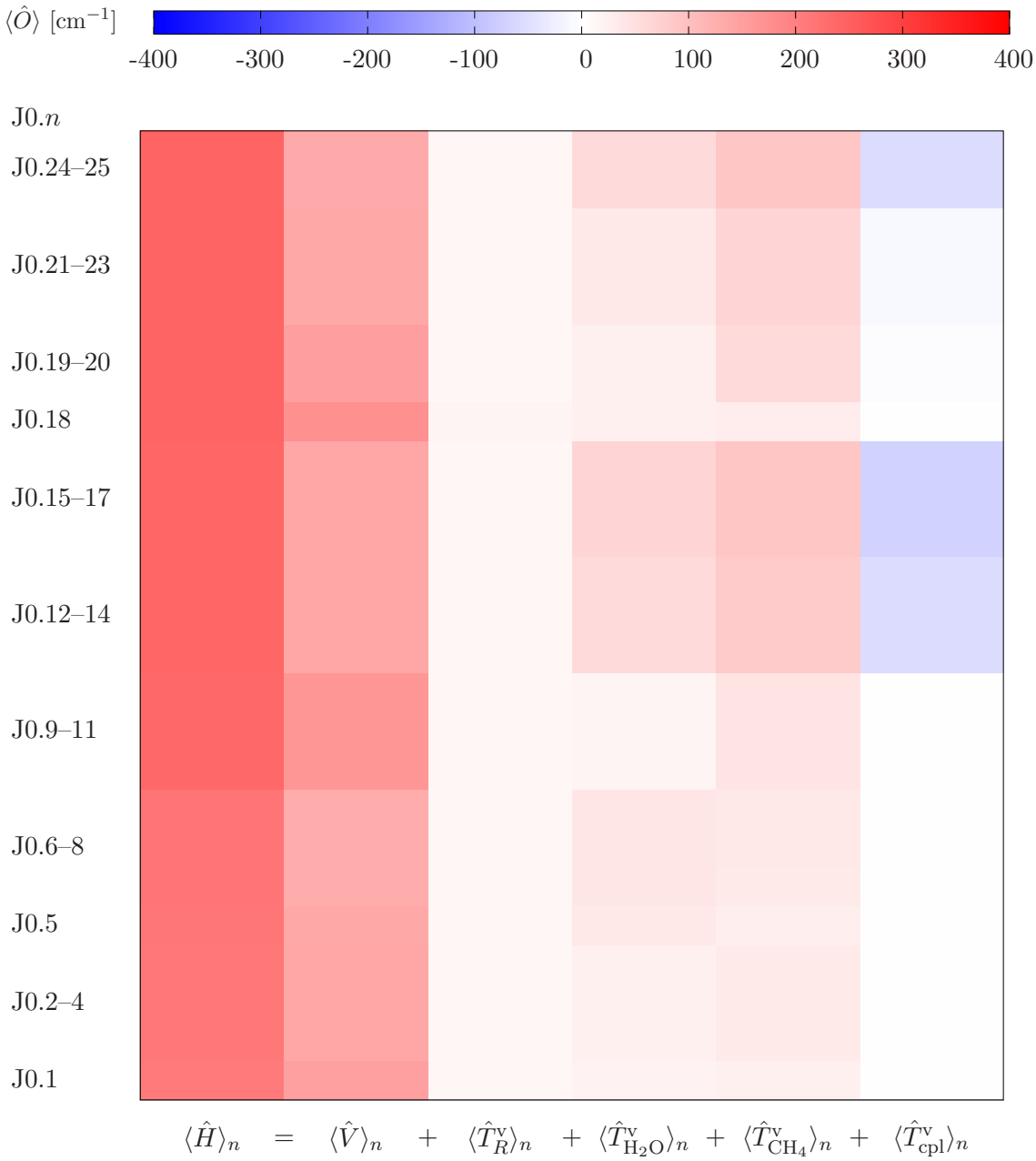

FIG. S3: Decomposition of the total vibrational energy among the different terms of the Hamiltonian for the first 25 $J = 0$ vibrational states of the CH_4·H_2O dimer.

can also enhance our understanding of the contributions of the various terms. For example, in Figure S3, we can observe that $\langle \hat{T}^{(\mathrm{v})}_{\mathrm{H_2O}} \rangle$ provides larger contributions to the ortho states than to the para states, which qualitatively indicates that the water moiety has larger (internal) rotational energy in the ortho levels than in the corresponding para levels (compare, for example, J0.1 and J0.5 in Figure S3).

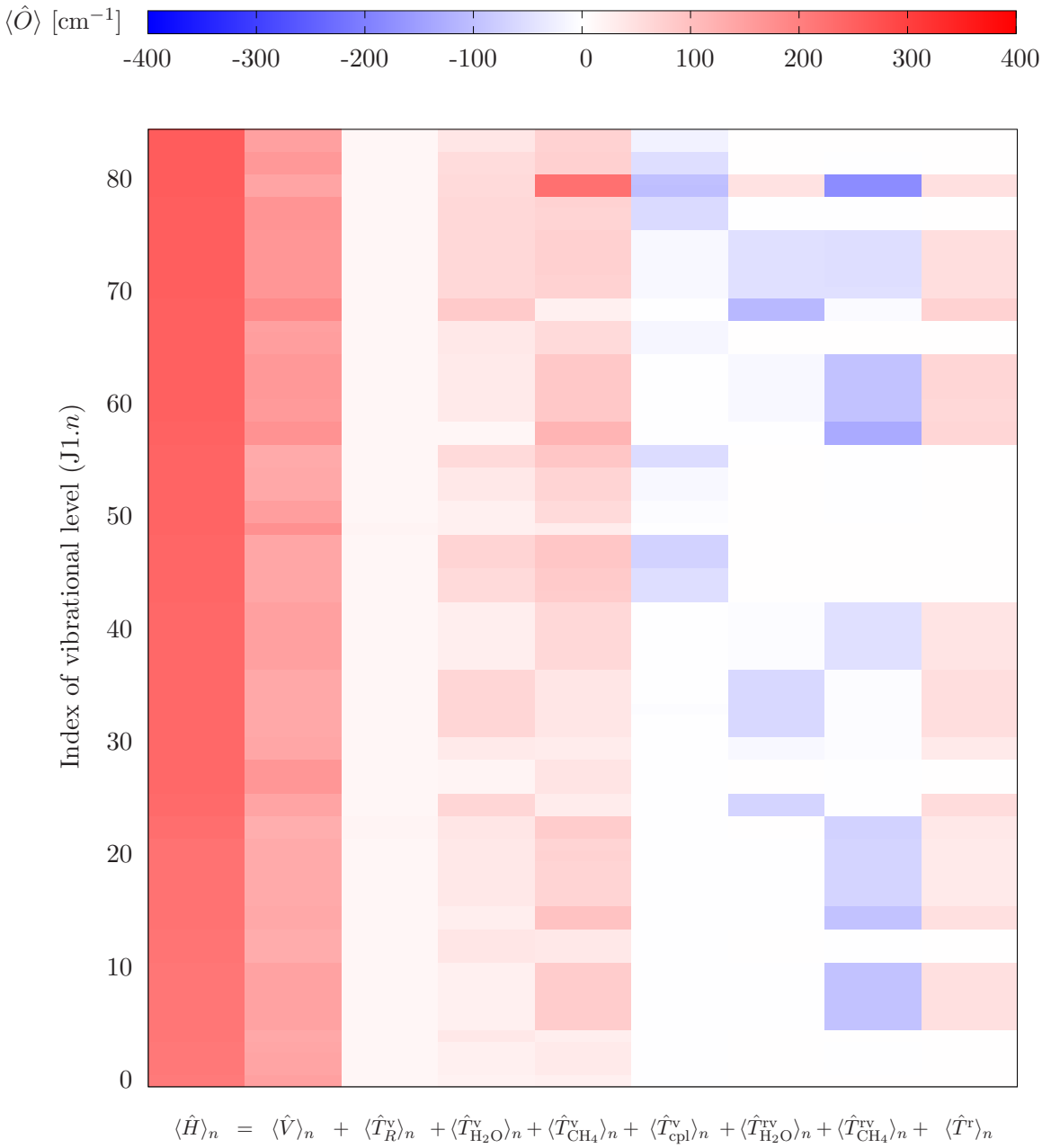

FIG. S4: Decomposition of the total rovibrational energy among the different terms of the Hamiltonian for the first 80 $J = 1$ rovibrational states of the CH_4·H_2O dimer (the $\langle \hat{T}^{\rm rv}_R \rangle_n$ contribution is zero, not shown).

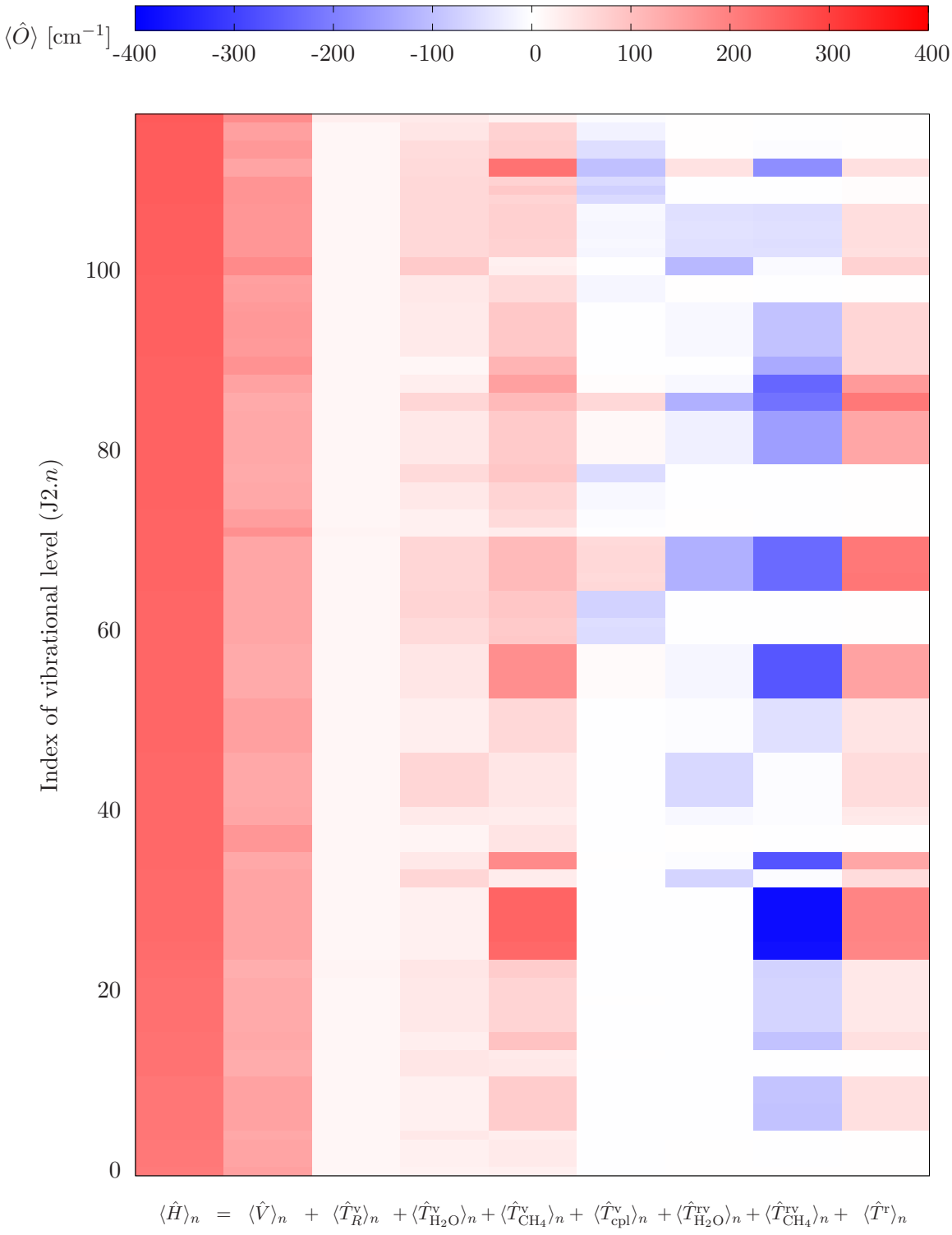

FIG. S5: Decomposition of the total rovibrational energy among the different terms of the Hamiltonian for the first 120 $J = 2$ rovibrational states of the CH_4·H_2O dimer (the $\langle \hat{T}^{\rm rv}_R \rangle_n$ contribution is zero, not shown).

S5. SELECTED DVR PLOTS

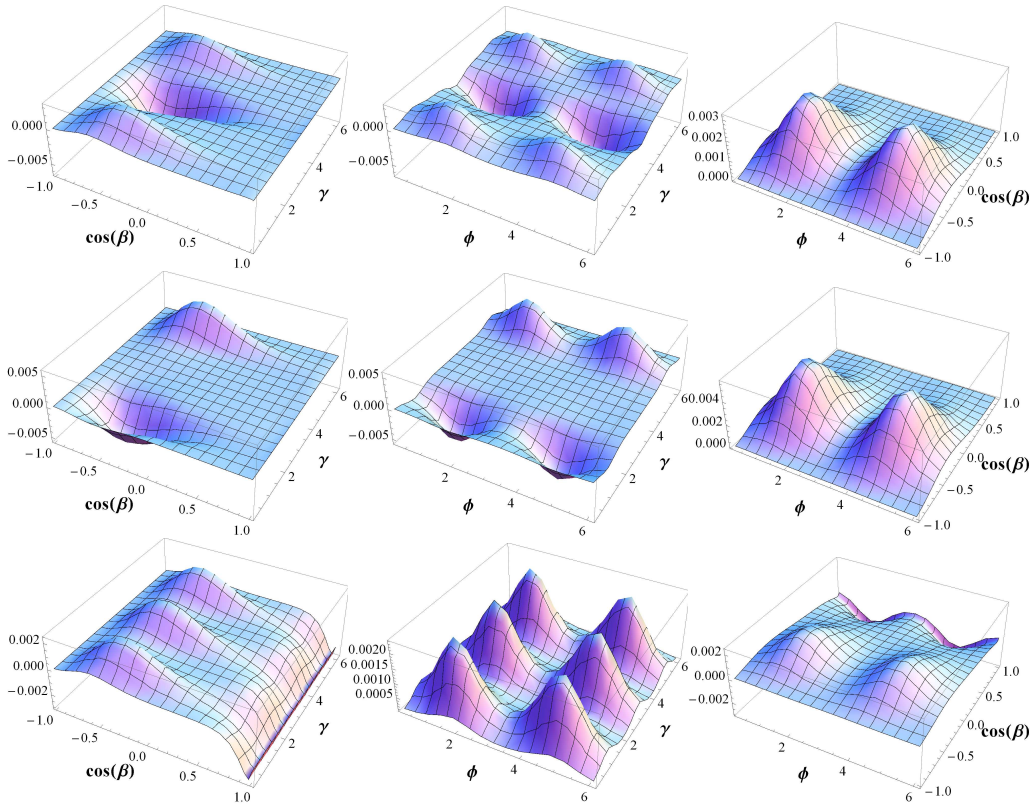

FIG. S6: Two-dimensional ($\cos\beta$–γ; ϕ–γ; ϕ–$\cos\beta$) cuts of the six-dimensional vibrational wave functions in DVR of the first set of triple-degenerate states, (4.8 cm^{-1}, J0.2–4) of CH_4·(para-H_2O).

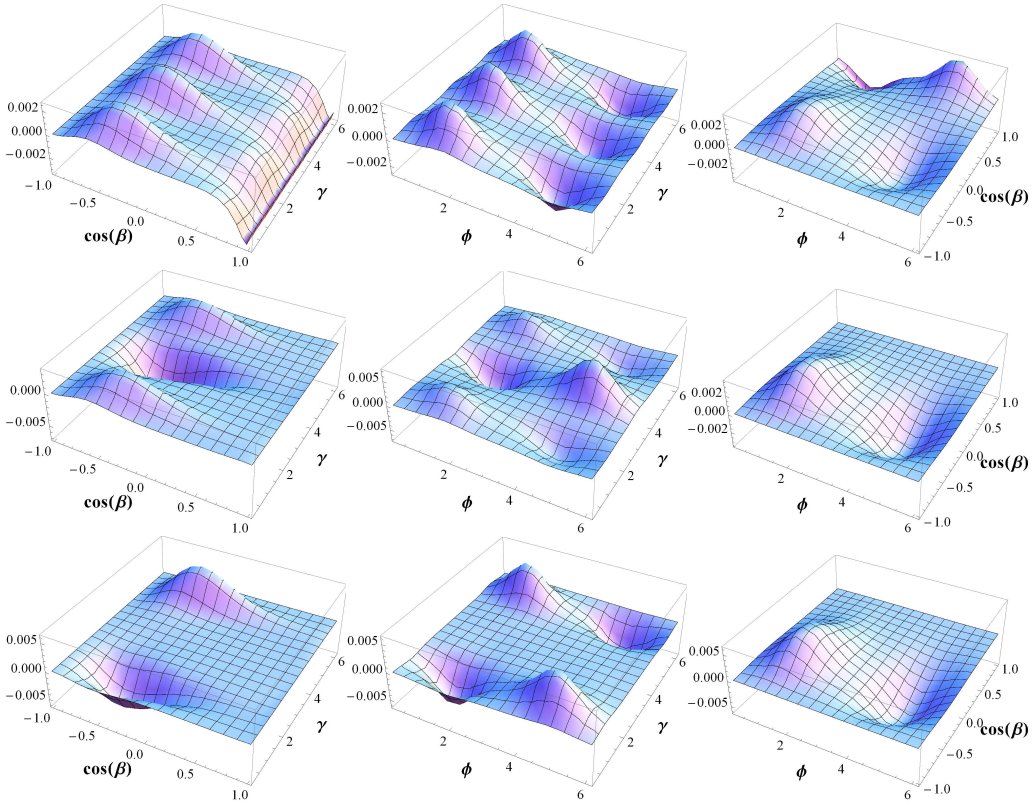

FIG. S7: Two-dimensional ($\cos\beta$–γ; ϕ–γ; ϕ–$\cos\beta$) cuts of the six-dimensional vibrational wave functions in DVR of the first set of triple-degenerate states, (11.2 cm^{-1}, J0.6–8) of CH_4·(ortho-H_2O).

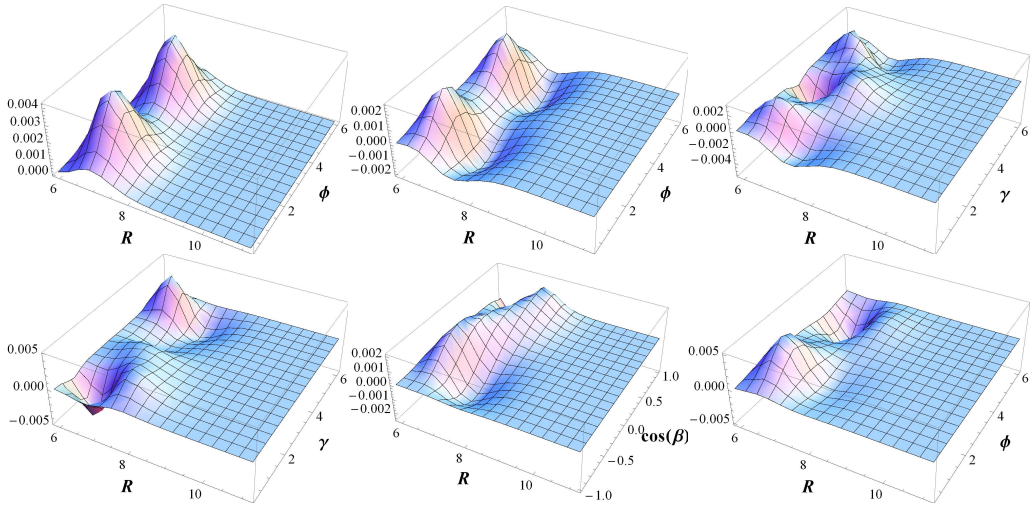

FIG. S8: Selected two-dimensional cuts of the six-dimensional vibrational wave functions in DVR. Top: J0.1, J0.36, and J0.40, bottom: J0.41, J0.42, J0.43.

[1] T. R. Dyke, J. Chem. Phys. **66**, 492 (1977).

[2] L. Dore, R. C. Cohen, C. A. Schmuttenmaer, K. L. Busarow, M. J. Elrod, J. G. Loeser, and R. J. Saykally, J. Chem. Phys. **100**, 863 (1994).

[3] J. T. Hougen, Methane Symmetry Operations, http://www.nist.gov/pml/pubs/methane/index.cfm (last accessed 22 April 2016).

[4] P. R. Bunker and P. Jensen, *Molecular symmetry and spectroscopy, 2nd Edition* (NRC Research Press, Ottawa, 1998).

[5] O. Akin-Ojo and K. Szalewicz, J. Chem. Phys. **123**, 134311 (2005).

[6] C. Qu, R. Conte, P. L. Houston, and J. M. Bowman, Phys. Chem. Chem. Phys. **17**, 8172 (2015).

[7] G. Brocks, A. van der Avoird, B. T. Sutcliffe, and J. Tennyson, Mol. Phys. **50**, 1025 (1983).